Materials Research. 2018; 21(3): e20171015
DOI: http://dx.doi.org/10.1590/1980-5373-MR-2017-1015

Physiochemical and Optical Properties of GdF_3:Pr@LaF_3@SiO_2 Microspheres

Anees Ahmad Ansari[a]*, Mohamed Aslam Manthrammel[b]

[a]*King Abdullah Institute for Nanotechnology, King Saud University, Riyadh-11451, Saudi Arabia*
[b]*Department of Physics, King Khalid University, Abha, 61413, Saudi Arabia*

Received: November 17, 2017; Revised: January 22, 2018; Accepted: February 19, 2018

The polyol-based co-precipitation process was employed for synthesis of GdF_3:Pr (core) and GdF_3:Pr@LaF_3 (core-shell) microspheres (MSs). Subsequently, an amorphous silica layer was deposited surrounding the core-shell MSs, which was verified from high-resolution transmission electron microscopy (TEM), energy dispersive X-ray analysis (EDX) and FTIR results. The absorption spectral results revealed the high solubility with good colloidal stability in aqueous solvents. The detailed structural and morphological analysis, as well as crystallinity of the samples, was investigated through X-ray diffraction, TEM and band gap energy results. The experimentally calculated band gap energy was found to decrease after gradually coating insulating layers of LaF_3 and amorphous silica over the surface, because of an effective increase in particle size. The Pr^{3+}-doped GdF_3 shows sharp $4f^15d^1 \rightarrow 4f^2$ emission bands (260-480 nm) as well as typical $4f^2 \rightarrow 4f^2$ emission lines (460-800 nm) of Pr^{3+} under $4f^2 \rightarrow 4f^15d^1$ excitation. After surface coating, comparative photoluminescence properties of the MSs were investigated by excitation and emission spectra. The origin of the different types of emission transitions were analyzed in details.

Keywords: *Praseodymium, Gadolinium fluoride, Core-shell, Silica, Band gap energy, Photoluminescence.*

1. Introduction

GdF_3 nanoparticles (NPs) as an important member of the lanthanide fluoride compounds (LnF_3) that possess very low phonon frequencies of crystal lattices and high radiative transition rate are regarded as a kind of excellent host materials for upconversion as well as down conversion photoluminescence[1-4]. Additionally, GdF_3 can also act as a highly efficient host lattice that achieves multicolor luminescence by varying the dopants since the gadolinium ion (Gd^{3+}) is a good intermediate that migrates and transfers energy[5-7]. Gadolinium fluoride is known as a multifunctional agent because it has lower vibrational energies than oxides, and consequently, the quenching of the excited state of the Ln actions is minimized, resulting in a higher quantum efficiency of the luminescence[7-9]. Besides, Gd^{3+} is an ideal paramagnetic relaxation agent used in magnetic resonance imaging because of its large magnetic moment and nanosecond time scale electronic relaxation time[7,9]. Hence, Gd^{3+}-based compounds are good candidates as multifunctional agents for multimodal bioimaging[8,10]. Presently, some efforts have been dedicated to preparing nano/micro GdF_3 crystals[1,9]. Zhang and co-workers have synthesized raisin-like GdF_3 nanocrystals by microwave method[5,11]. Lin and coworkers synthesized GdF_3 spindle-like structures via microwave-assisted ionic liquid method[5,12]. Chen and co-workers prepared GdF_3 NPs through a one-step solvothermal route by employing poly(acrylic acid) as a capping agent[8]. Yin et al. have obtained GdF_3 NPs with polyvinyl pyrrolidone as a surfactant and found that the doping of Li^+ could enhance the red emission from GdF_3:Yb^{3+}, Er^{3+} [6].

In order to preserve the high luminescent quantum efficiency of the luminescent nanomaterials, Yi et al. initially reported the synthesis of a core-shell structure composed of $NaYF_4$:Yb^{3+}/Er^{3+}@$NaYF_4$ and $NaYF_4$:Yb^{3+}/Tm^{3+}@$NaYF_4$, and showed reduced interactions of lanthanides with surface defects, ligands, and solvent[13,14]. As a result, the emission intensity enhanced up to 29 times when a shell was deposited on upconverting $NaYF_4$:Yb^{3+}/Tm^{3+}@$NaYF_4$ core NPs. The Even higher increase, up to 450 times, was reported by Wang et al. for shell covered small NPs (10 nm)[15]. Additionally, more complex shell compositions (e.g., $NaYF_4$:Yb/Er@$NaYF_4$, $NaGdF_4$:Yb/Er@$NaGdF_4$, $NaYF_4$:Ce/Tb@$NaYF_4$, LaF_3:Nd@LaF_3, $CaMoO_4$:Ln @$CaMoO_4$, YF_3:Ln@LaF_3, CaF_2:Ce/Tb, etc.) were also proposed to achieve further increase in the photoluminescence intensity[10,14,16-28]. However, due to the weak solubility of these core-shell NPs in aqueous or non-aqueous solvents, their application in photonic based bio-application is limited. Therefore, further surface modifications of the micro/NPs are required before they can be used for biological applications. Moreover, surface structure of the nanomaterials is likely to provide a better environment for attachment of desired bio-macromolecules

*e-mail: aneesaansari@gmail.com

(antibody or oligonucleotides), leading to increased loading of bio-macromolecules. But, it is still a great challenge to directly synthesize water-soluble luminescent-doped lanthanide NPs with the desired optical properties. Therefore, it is very important need to synthesize water-soluble, biocompatible and non-toxic luminescent activator-doped lanthanide NPs; otherwise, their use in bio-related applications is very limited. Recently, some synthesis routes have been developed to selectively prepare the luminescent ion doped lanthanide nanomaterials, including co-precipitation method[29], hydrothermal treatment[30-33], thermal decomposition reaction of the corresponding lanthanide compound precursors (e.g., lanthanide oleate, lanthanide trifluoroacetate) in high boiling solvents such as 1-octadecenceat high temperature by using oleic acid or oleylamine as a capping agent[34-37], solid-state reaction as well as reversed micelle method[38], and as a result, a series of the GdF_3 NPs with specific morphologies and tunable luminescence properties were obtained[3,5].

To the best of our knowledge, there is no report on the synthesis of Pr^{3+} doped GdF_3 and their surface covered micro/NPs. Herein, we employ a simple polyol based co-precipitation process to prepare Pr^{3+} ion doped GdF_3 (core) and an insulating layer coated GdF_3:Pr@LaF_3 core-shell MSs. Subsequently, these core-shell microstructures were encapsulated with aqueous soluble amorphous silica layer through sol-gel method. The crystal structure, crystallinity, and morphology of core as well as their surface coated core-shell MSs were investigated by X-ray powder diffraction (XRD) and Transmission electron microscopy (TEM). In the present study, we carried out a detailed investigation of the optical properties of core-MSs and compared their results with surface coated core-shell and amorphous silica coated core-shell-SiO_2 MSs, which are an excellent probe to a local crystal structure. Additionally, we proposed co-relation between band gap energy and grain size of the as-prepared core and their subsequent LaF_3 and amorphous silica shell coated MSs. The growth of an inert LaF_3 shell on the surface of GdF_3:Pr core MSs suppresses non-radiative recombination processes at the MSs surface, which is important for producing high quantum yield photoluminescence. However, photoluminescence efficiency of silica surface modified core-shell-SiO_2 MSs were quenched with respect to core-shell MSs due to nonradiative energy losses enhanced by the surface passivation (caused by the presence of high energy water molecules or organic moieties etc.) molecules. Our results clearly show that the silica surface modified core-shell-SiO_2 MSs exhibit good water dispersibility and colloidal stability in aqueous solvents. Finally, it is well-known that the silica surface modification of the micro/NPs is an important method for solubility, biocompatibility and their conjugation with bio-macromolecules, which could be employed as a promising multifunctional macro/nano platform for simultaneous photonic based bio-imaging and bio-probe etc.

2. Experimental Procedure

2.1. Materials

Gadolinium oxide (99%, BDH chemicals Ltd, England), lanthanum oxide (99%, BDH chemicals Ltd, England) Praseodymium oxide (99.99%, Alfa Aesar, Germany), ethanol (E-Merck, Germany), Tetraethyl orthosilicate (TEOS, 99 wt% analytical reagent A.R.), ethylene glycol(EG), NH_4F, HNO_3 and NH_4OH were used as the starting materials without any further purification. $Gd(NO_3)_3.6H_2O$, $Pr(NO_3)_3.6H_2O$ and $La(NO_3)_3.7H_2O$ were prepared by dissolving the corresponding oxides in diluted nitric acid. The de-ionized water was prepared using a Milli-Q system (Millipore, Bedford, MA, USA).

2.2. Preparation of GdF_3:Pr^{3+} MSs

For the preparation of GdF_3:Pr^{3+} MSs ($Gd_{0.99}Pr_{0.01}F_3$), 0.2 M stock solutions of $Gd(NO_3)_36H_2O$ and $Pr(NO_3)_36H_2O$ were prepared in deionized water at normal pH[6,7]. Briefly, 9.9 ml of $Gd(NO_3)_36H_2O$ and 0.1 ml of $Pr(NO_3)_36H_2O$ were dissolved in 50 ml EG at normal pH. Then an equal molar aqueous solution of NH_4F(1.7 g) was added dropwise under magnetically stirred reaction, and the whole solution was kept on hot plate with magnetic stirring at 80°C. This homogeneously mixed solution was transferred into a 250 ml round bottle flask fitted with reflux condenser and reaction continued for 4 h until complete precipitation. On cooling to room temperature, the white precipitates got segregated to the bottom. The product was collected by centrifugation and washed with distilled water and absolute ethanol several times, and dried in an oven at 60 °C for 6 h. The obtained solid product can be re-dispersed in deionized water to form a water-dispersible solution.

2.3. Preparation of GdF_3:Pr^{3+}@LaF_3 Core-shell MSs

For the preparation of GdF_3:Pr^{3+}@LaF_3 core-shell MSs, similar polyol process was used as discussed above. The as-prepared 0.500 g GdF_3:Pr^{3+} was dispersed with the help of ultra-sonication in 10 ml of distilled water. This dispersed MSs solution was mixed into magnetically stirred hot ethylene glycol dissolved $La(NO_3)_37H_2O$ (0.500 g) solution. After thirty minutes an equal. a molar aqueous solution of $NH_4F$was injected into the foregoing mixed system under magnetic stirring at 80 °C. Afterward, this suspension was refluxed at 80 °C for 3 h until the complete precipitation occurs. This white precipitate was centrifuged and washed many times with ethanol and dist. water to remove excess unreacted reactants. The core-shell MSs were collected after centrifugation and allowed to dry in ambient temperature for further characterization.

2.4. Preparation of Silica-Coated GdF_3:Pr^{3+}@ LaF_3@SiO_2 Core-shell MSs

The GdF_3:Pr^{3+}@LaF_3@SiO_2 core-shell MSs were prepared through a versatile solution sol-gel method as follows (20, 39, 40). The synthesized GdF_3:Pr^{3+}@LaF_3 MSs (50 mg) were well dispersed in a mixed solution of deionized water (50 mL), ethanol (70 mL) and aqueous ammonia (1.0 mL) in a flask. Afterward, 1.0 mL of tetraethylorthosilicate (TEOS) was added dropwise over 2 min, and the reaction was allowed to proceed for 6-7 h under continuous mechanical stirring. After continuous stirring at room temperature, the silica-coated GdF_3:Pr^{3+}@LaF_3 core-shell MSs were separated by centrifugation, washed several times with ethanol and dried at room temperature for further analysis.

2.5. Characterization

The crystallinity and phase purity of the powder samples were examined by Powder X-ray diffraction (XRD, Rigaku X-ray diffractometer) at room temperature equipped with Ni filter using *Cu-Kα*(λ=1.5405Å) radiation as a X-ray source. Morphology and elemental analysis were carried out using Field emission transmission electron microscope (FE-TEM) equipped with the Energy dispersive X-ray (EDX) (JEM-2100F, JEOL, Japan). FTIR spectra were recorded by Vertex 80 (Bruker, USA) spectrophotometer using KBr pellet technique. UV/Vis spectra were recorded by Cary 60 optical absorption spectrophotometer. The excitation and emission spectra were recorded by Fluorolog 3 spectrometer (model: FL3-11), Horiba JobinYvon Edison MJ USA.

3. Results and Discussion

3.1. Crystal Phases and Morphologies of the Microspheres

The phase purity, crystal structure, composition and crystalline nature of the prepared products were first examined by XRD. Fig.1 reveals that all samples are well crystalline and reflection planes readily indexed to orthorhombic phase (Space group: *Pnma*), which are in good agreement with the standard data of bulk GdF_3 (ICDD# 49-1804)[3,7,9]. As illustrated in Fig.1b, the reflection peaks in core-shell MSs become sharp with respect to core-MSs; could be due to inert crystalline LaF_3 shell deposition which enhances the grain size of the material. Furthermore, the reflection planes are broadened with decreased relative peak intensity in the case of core-shell-SiO_2 MSs as seen in Fig.1c. It indicates that the silica network formed on the surface of crystal expanded the nanopore structure and rearranged the Si-O-Si network structures without any impurities [21,24,39,42]. The observed broadening or slightly shifting in diffraction peaks in the case of core-shell-SiO_2 MSs are mainly due to particle size effect, instrumental or strain

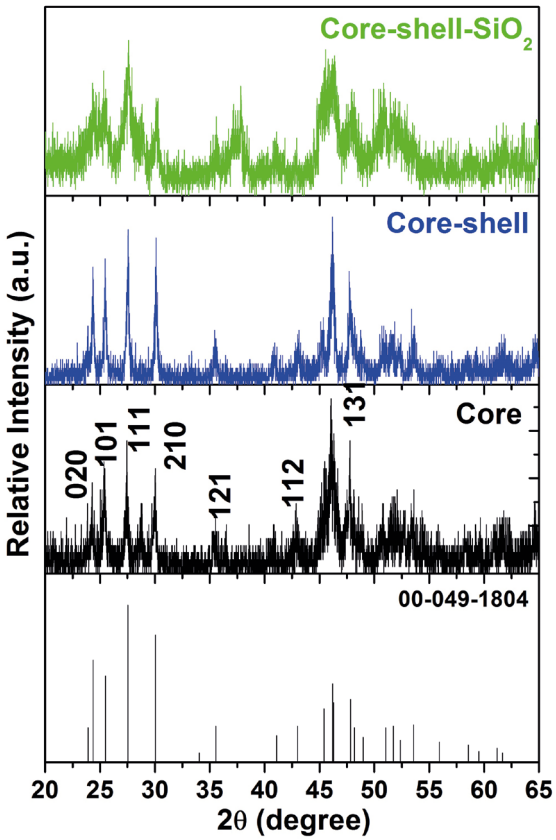

Figure 1. X-ray diffraction pattern of core, core-shell and core-shell-SiO_2 microspheres.

broadening. However, no defined characteristic peak for silica was observed after one coating process due to the thinner property of the silica layer.

Transmission electron microscopy was used to estimate the size and morphological changes after surface modification as well as the thickness of the shell around the core-MSs. As seen in low magnification TEM image in Fig.2a, the particles are well dispersed irregular spherical shaped porous microspheres with the average particle size 200-400 nm. As shown in Fig.2c&d, a thin but silica layer, with a thickness of ~10 nm has been effectively coated surrounding the core-shell structure. To confirm this hypothesis we utilized SAED and EDX analysis. The crystalline nature and orthorhombic crystal lattice of the core-shell-SiO_2-MSs were also confirmed from selected area electron diffraction (SAED) pattern (Fig.2b). In the SAED pattern, the strong concentric ring patterns can be indexed to the (101), (111), (210), (112) and (131) planes of the orthorhombic GdF_3 phase and demonstrate its crystalline nature[4,7,41]. The EDX analysis indicates that the single core-shell-SiO_2-MSs is composed of Gd, La, Pr, F,O and Si elements. Thus it is confirmed that silica has been successfully grafted on the surface of core-shell MSs. No other impurity peak was detected indicating the phase purity of the material supporting the XRD results.

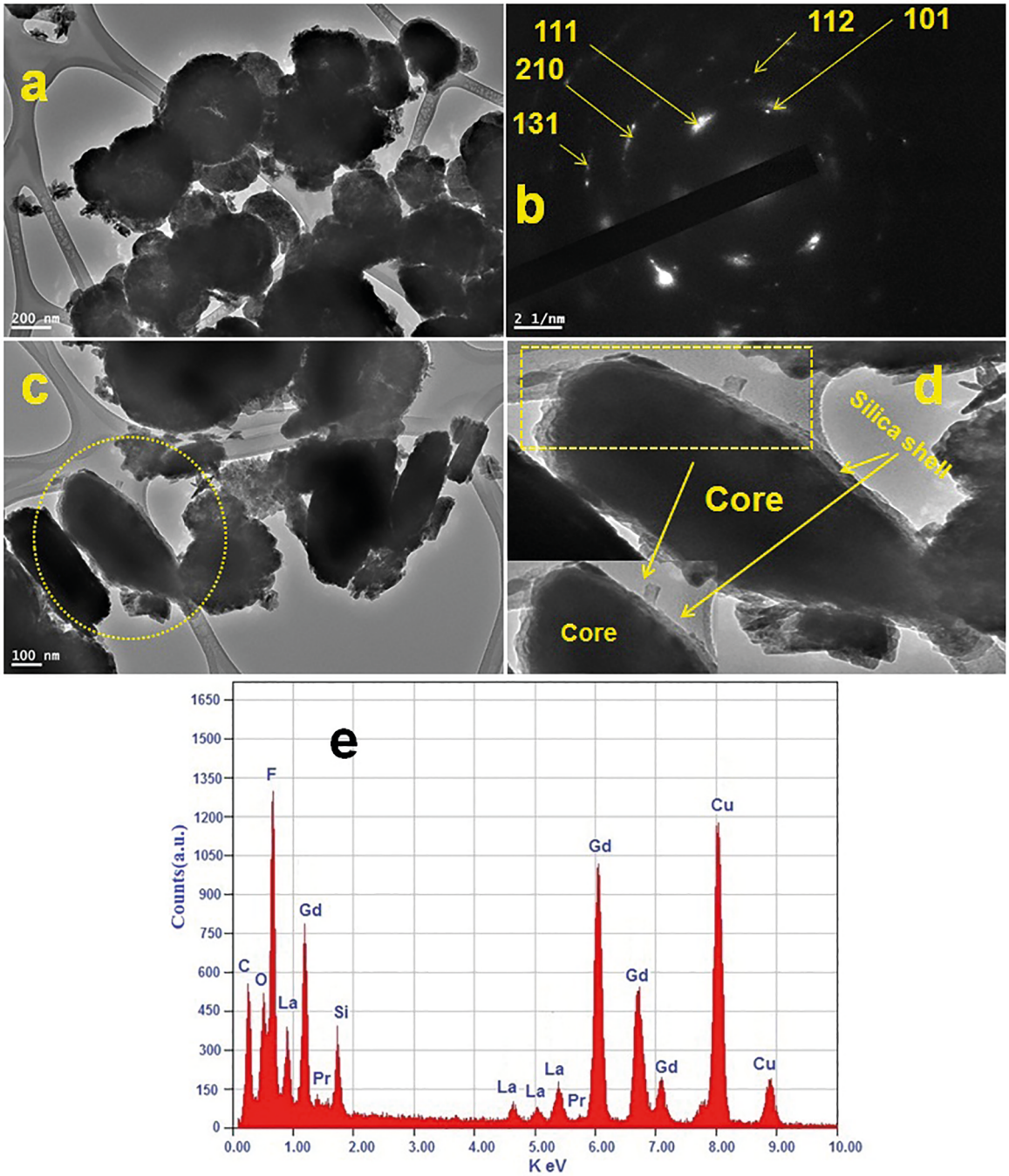

Figure 2. FETEM images of (a) core microspheres (b) SAED (c&d) core-shell-SiO_2 microspheres and (e) Energy dispersive X-ray analysis of core-shell-SiO_2 microspheres.

Thermogravimetric analysis was carried out to examine the thermal stability of the core, core-shell, and core-shell-SiO_2-MSs (Fig.3). The thermograms of core and core-shell MSs exhibit two-stage weight losses. In the first stage of core and core-shell MSs approximately 2.5 mol% weight loss took place in between 25-450 °C, which correspond to the crystalline water or organic moieties which are bonded with MSs in different bonding state for the present complex system. The second stage core and core-shell MSs showed a minor weight loss of about 1.5 mol% and 3 mol% in the temperature range of 450-900 °C which is attributed to the combustion of carbonates linked with Gd^{3+} ion. However, in core-shell-SiO_2 MSs a slow moving decomposition (~ 12 mol% weight loss) is observed in the temperature range 25-900 °C. It could be due to slow removal of water molecules followed by combustion of surface amorphous silica transforming it into silicate. This hypothesis is also supported by FTIR analysis.

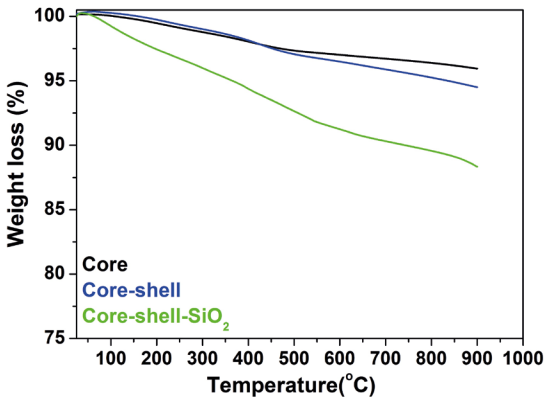

Figure 3. Thermogravimatric analysis of the core, core-shell and core-shell-SiO_2 microspheres.

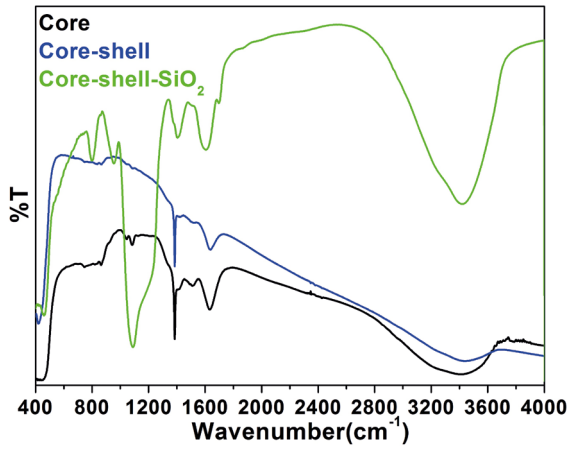

Figure 4. FTIR spectra of the Core, core-shell and core-shell-SiO_2 nanocrystals.

FTIR spectral measurements were carried out to verify the surface chemistry of the prepared samples. As seen in Fig. 4, FTIR spectra reveal a diffused band before and after surface modification located at 3412 cm^{-1}, which originate from O-H asymmetric and symmetric stretching vibration of the anchored physically adsorbed residual water molecules on the surface of MSs[40,42,43]. Two additional bands found at around 1634 and 1384 cm^{-1} are attributed to the bending and wagging vibrations of -OH groups[43]. The broadening of this stretching vibration indicates that large numbers of -OH groups either chemically bonded or physically adsorbed are present on the surface of MSs. It is worth mentioning that, MSs are prepared in aqueous media and their surface may be covered by -OH groups. An observed infrared absorption band at around 460 cm^{-1} in core and core shell MSs is assigned to asymmetric bending vibrational modes of F-Gd-F bonding. The silica surface encapsulation is confirmed by observed characteristic peaks located at 1080, 950, 793 and 460 cm^{-1} ascribed to the symmetric stretching and bending vibration modes of amorphous silica ((Si-O), (Si-O-Si), and (Si-OH)), which are in good agreement with the TEM and EDX observed results[39,42,44]. It indicates that amorphous silica has been grafted successfully around the surface of core-shell MSs which makes them high soluble in aqueous solvents.

Figure 5 shows the absorption spectra of core, core-shell and silica surface modified core-shell-SiO_2 MSs measured in dist. water over the range from 200-600 nm within UV-Visible region. As observed from FTIR spectra, the surface of MSs are covered with -OH groups which make them water-dispersible, whereas, the formed aqueous dispersion is not stable enough and precipitation could be clearly observed after 24 h because of the low contents of the hydrophilic components on the surface of the core and core-shell MSs. In order to improve their dispersibility along with colloidal stability, we modified the surface of core-shell with amorphous silica. Silica surface had a lot of hydroxyl groups (hydrophilic group), which are easily available for covalent interaction with the aqueous solvent or for conjugation with bio-macro-molecules. As observed in Fig.5A, the absorption spectrum of silica modified MSs reveals a significant enhancement in absorption edge with respect to non-modified MSs. It suggests that the optically active silica has been effectively grafted around the surface of core-shell MSs which is also inconsistent with the FTIR results. It is worth mentioning that the well-known 4*f*-4*f* absorption transitions of Pr^{3+} ions are not detected in these nano phosphor samples causing the small quantity of the Pr^{3+} ion in the host lattice. We observed a similar trend in absorption spectra recorded in absolute ethanol as seen in Fig. 5B. Optical absorption spectra were utilized to reveal the correlation between band gap energy and particle size of the as-prepared materials. According to the Tauc law[45], the quantitative evaluation of the energy band gap can be performed by plotting $(\alpha h\nu)^2$ versus photon energy ($h\nu$) and extrapolating the linear part of the curve to the energy axis as shown in inset Fig.5A &B. The energy band gap for core, core-shell, and core-shell-SiO_2 MSs are found to be 2.22, 2.54 and 2.01 eV in H_2O and 1.84, 2.27 and 1.72 in absolute ethanol, respectively. The reduction in band gap energy after surface coating could be related to grain size of the material. Owing to the shell formation crystallinity decreases because of increase in grain size of the material.

Photoluminescence spectra verified the Pr^{3+} doping into the GdF_3 crystal lattice. Fig. 6 illustrates the excitation spectra of core, core-shell and core-shell-SiO_2 MSs by monitoring the emission at 486 nm ($^3H_4 \rightarrow {}^3P_0$) at room temperature. The sharp excitation transitions between 280 -480 nm are assigned to the $4f^2$-$4f^2$ intra-configuration forbidden transitions of Pr^{3+}. The observed excitation transitions at 296, 358, 444 and 467 nm correspond to the $4f \rightarrow 5d$, $^3H_4 \rightarrow {}^3P_2$ and $^3H_4 \rightarrow {}^3P_1, {}^1I_6$ transitions, respectively[46-49].

Fig.7 displays the emission spectra of samples obtained by excitation at 444 nm ($^3H_4 \rightarrow {}^3P_2$). Several sharp and some strong $4f^2 \rightarrow 4f^2$ emission transitions are clearly resolved, having maxima at 480, 486, 499, 520, 537, 584-597,

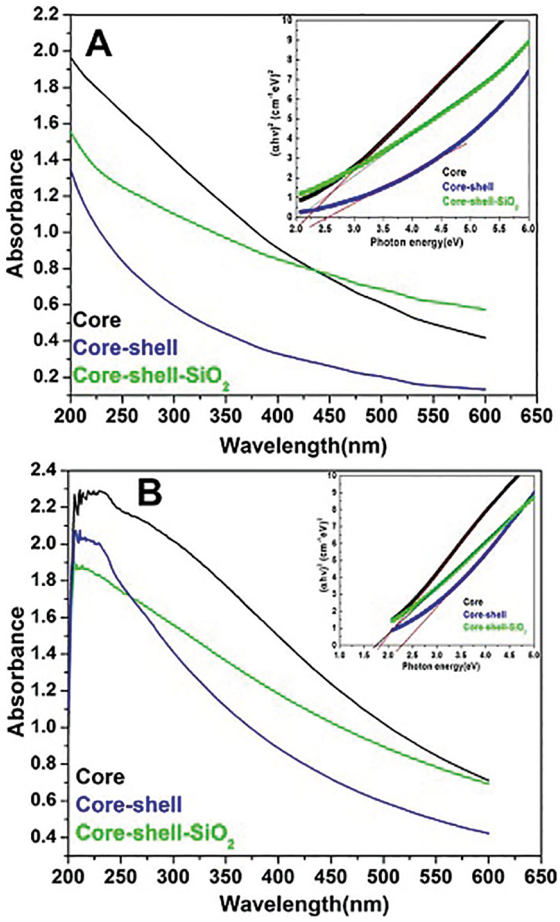

Figure 5. (A). UV-Vis absorption spectra of core, core-shell and core-shell-SiO_2 microspheres in de-ionized water and inset shows the plot of $(\alpha h\nu)^2$ vs. photon energy($h\nu$) of core, core-shell and core-shell-SiO_2 microspheres. (B). UV-vis absorption spectra of core, core-shell and core-shell-SiO_2 microspheres in absolute ethanol and inset shows the plot of $(\alpha h\nu)^2$ vs. photon energy($h\nu$) of core, core-shell and core-shell-SiO_2 microspheres.

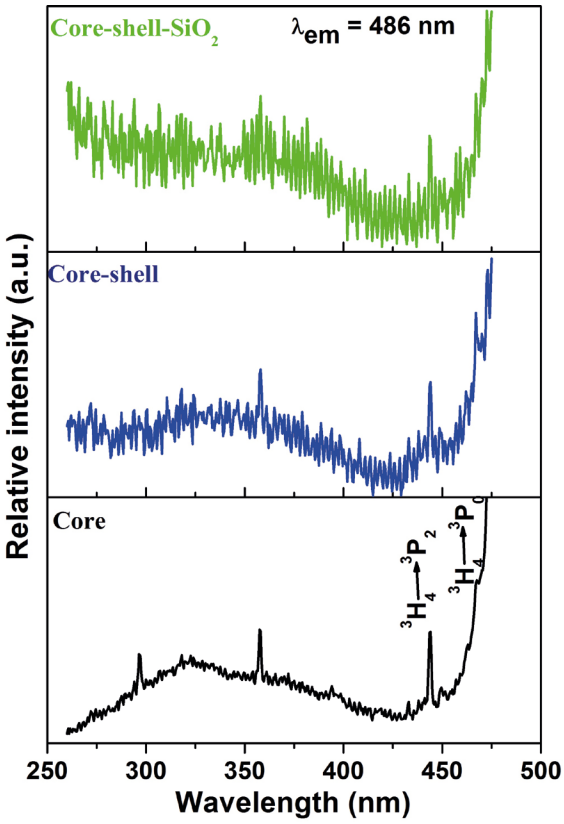

Figure 6. Excitation spectra of the core, core-shell and core-shell-SiO_2 microspheres.

600-612, 680, 691 and 727 nm assigned to $^3P_1 \rightarrow {}^3H_4$, $^3P_0 \rightarrow {}^3H_4$, $^3P_1 \rightarrow {}^3H_5$, $^3P_0 \rightarrow {}^3H_5$, $^3P_1 \rightarrow {}^3H_6$, $^1D_2 \rightarrow {}^3H_4$, $^3P_0 \rightarrow {}^3H_6$, $^3P_0 \rightarrow {}^3F_2$, $^3P_0 \rightarrow {}^3F_3$, and $^3P_0 \rightarrow {}^3F_4$ transitions of the Pr^{3+} ion, respectively[12,46,49,50]. There are two possible 4*f* emitting states for the Pr^{3+} ion, i.e. $^3P_0$ and $^1D_2$ levels, and the emission color of Pr^{3+} depends on the intensity ratio of $4f^2 \rightarrow 4f^2$ transitions at a fixed energy, which is strongly affected by the host lattice. The observed emission is typical characteristics of $4f^2 \rightarrow 4f^2$ rare earth transitions and is typical for Pr^{3+} in a fluoride environment. After relaxation from the $^3P_2$ to the $^3P_0$ levels, emissions are detected to the first six excited levels from 450 nm to 750 nm. As seen in Fig. 7, the strongest features of emission bands are located at 486, 604 and 727 nm, which are ascribed to the $^3P_0 \rightarrow {}^3H_4$, $^3P_0 \rightarrow {}^3H_6$ and $^3P_0 \rightarrow {}^3F_4$ transitions, respectively[49]. No transition originating from the $^1D_2$ state is clearly observed with excitation in the ^3P_J multiplets. Previously, some researchers observed emission, after excitation in the ultraviolet, from two different types of Pr^{3+} sites noted as (1) and (2) respectively: the first, Pr(1) is in a strong crystal field site, in low concentration, and the second, Pr(2) is a weak crystal field site with high concentration[12,47]. This latter type is ascribed to Pr^{3+} ions occupying the Gd^{3+} sites in GdF_3 and Pr(1) is ascribed to Pr^{3+} ions with a locally distorted coordination. In our case, the emission is in agreement with that observed after short-wavelength pumping in previous works and is attributed to Pr(2) sites. This means that no hints of lattice distortion or contaminants are present in the luminescence of Pr^{3+} in MSs.

As shown in Fig.7, a significant enhancement is observed in the emission spectra of core-shell MSs because of an insulating LaF_3 layer effectively grafted surrounding the luminescent core-MSs. Here the presence of LaF_3 shell protects the dopants in the core, especially those near the surface, from quenching arising from high energy hydroxyl groups and surface-bound ligands[19,34,51]. The presence of an undoped LaF_3 layer on the surface of luminescent core-MSs eliminates the non-radiative transition pathways and protects the core from light scattering effect. According to recent reports, the addition of an undoped LaF_3 shell on the surfaces of GdF_3:Pr core-MSs would eliminate the surface defects, which enhance the relative emission intensities of the material[19,21,51]. The reduction in quenching improves the overall quantum yield of the luminescent materials.

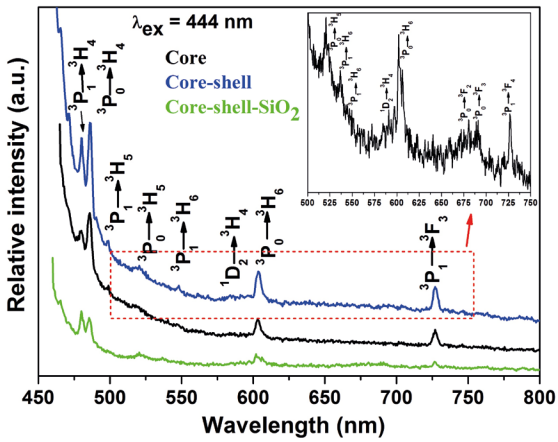

Figure 7. Emission spectra of the core, core-shell and core-shell-SiO_2 microspheres.

Furthermore, our group has shown strong evidence for the formation of core-shell lanthanide MSs using the fore mentioned synthesis procedure[19,24], and we conclude the same is true for this core-shell structure. Figure 8 depict the energy level program for trivalent praseodymium ion.

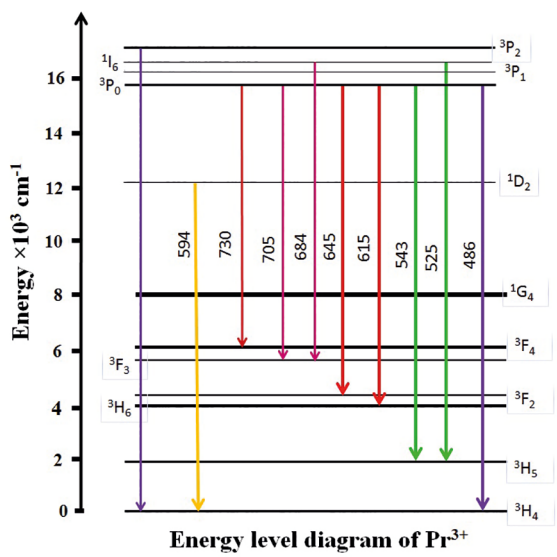

Figure 8. proposed energy level diagram of Pr(III) ion.

After the core-shell MSs are coated with amorphous silica layer their emission intensity decreased to some extent because of the light-scattering effect on both emission and incident light by the silica layer. The presence of free Si-OH groups on their surfaces not only results in high solubility in water, but also allows further conjugation with various biomolecules, which paves the way for further bio-applications of the core-shell-SiO_2 MSs. However, these Si-OH groups may also cause considerable non-radiative transition and reduce the quantum yield of fluorescence emission of lanthanide ions[52-56]. The effect of hydroxyl groups on the fluorescence emission of lanthanide ions in the MSs was investigated. To investigate the location of the hydroxyl groups in the MSs, Pr^{3+} was used as a probe because the fluorescence of Pr^{3+} ion is very sensitive to their immediate surroundings.

4. Conclusion

In summary, we proposed a strategy to enhance the emission intensity with colloidal stability in aqueous solvents by gradually coating undoped LaF_3 and amorphous silica shell surrounding the luminescent ion doped GdF_3:Pr core-MSs. The results show that the emission intensity of luminescent core-MSs was significantly increased after core-shell formation, but decreased after amorphous silica surface coating due to surface silanol (Si-OH) groups scattered the emission and incident light from the surface of core-shell MSs. However, these Si-OH groups improve the solubility and colloidal stability in aqueous and non-aqueous solvents as confirmed by UV/Vis results. TEM images showed the successful silica surface coating which was verified by EDX and FTIR results. The emission spectra exhibited emission peaks associated with the electronic energy inter-level transitions of the Pr^{3+} ion. The results of emission spectra showed that the excitation process by high energy photons the self-trapped excitons were created with an energy that is resonant to ^3P_J (J = 0, 1, 2) and $^1I_6$ levels and high enough to populate them. Emission spectra were observed in the wavelength range associated with the three basic colors: blue color due to the contributions of the GdF_3 host and Pr^{3+} ion and the green and red colors due to the Pr^{3+} ion.

5. Acknowledgement

Author is thankful for the financial support to the King Abdullah Institute for Nanotechnology, Deanship of Scientific Research, King Saud University, Riyadh, Saudi Arabia.

6. References

1. Evanics F, Diamente PR, van Veggel FCJM, Stanisz GJ, Prosser RS. Water-soluble GdF_3 and GdF_3/LaF_3 Nanoparticles - Physical Characterization and NMR Relaxation Properties. *Chemistry of Materials*. 2006;18(10):2499-2505.

2. Zhao Q, Shao B, Lü W, Jia Y, Lv W, Jiao M, et al. Doping alkaline-earth: a strategy of stabilizing hexagonal GdF_3 at room temperature. *Dalton Transactions*. 2013;42(43):15482-15488.

3. Zhao Q, Lü W, Guo N, Jia Y, Lv W, Shao B, et al. Inorganic-salt-induced morphological transformation and luminescent performance of GdF_3 nanostructures. *Dalton Transactions*. 2013;42(19):6902-6908.

4. Tian Y, Tian J, Li X, Yu B, Shi T. Facile synthesis of ultrasmall GdF_3 nanowires *via* an oriented attachment growth and their luminescence properties. *Chemical Communications*. 2011;47(10):2847-2849.

5. Li C, Ma P, Yang P, Xu Z, Li G, Yang D, et al. Fine structural and morphological control of rare earth fluorides REF_3 (RE = La-Lu, Y) nano/microcrystals: microwave-assisted ionic liquid synthesis, magnetic and luminescent properties. *CrystEngComm*. 2011;13(3):1003-1013.

6. Yin W, Zhao L, Zhou L, Gu Z, Liu X, Tian G, et al. Enhanced Red Emission from GdF_3:Yb^{3+},Er^{3+} Upconversion Nanocrystals by Li^+ Doping and Their Application for Bioimaging. *Chemistry - A European Journal*. 2012;18(30):9239-9245.

7. Tian Y, Yang HY, Li K, Jin X. Monodispersed ultrathin GdF_3 nanowires: oriented attachment, luminescence, and relaxivity for MRI contrast agents. *Journal of Materials Chemistry*. 2012;22(42):22510-22516.

8. Ju Q, Liu Y, Tu D, Zhu H, Li R, Chen X. Lanthanide-Doped Multicolor GdF_3 Nanocrystals for Time-Resolved Photoluminescent Biodetection. *Chemistry - A European Journal*. 2011;17(31):8549-8554.

9. Xu J, Gai S, Ma P, Dai Y, Yang G, He F, et al. Gadolinium fluoride mesoporous microspheres: controllable synthesis, materials and biological properties. *Journal of Materials Chemistry B*. 2014;2(13):1791-1801.

10. Chen GY, Ohulchanskyy TY, Liu S, Law WC, Wu F, Swihart MT, et al. Core/Shell $NaGdF_4$:Nd^{3+}/$NaGdF_4$ Nanocrystals with Efficient Near-Infrared to Near-Infrared Downconversion Photoluminescence for Bioimaging Applications. *ACS Nano*. 2012;6(4):2969-2977.

11. Wang S, Su S, Song S, Deng R, Zhang H. Raisin-like rare earth doped gadolinium fluoride nanocrystals: microwave synthesis and magnetic and upconversion luminescent properties. *CrystEngComm*. 2012;14(13):4266-4269.

12. Lecointre A, Bessière A, Bos AJJ, Dorenbos P, Viana B, Jacquart S. Designing a Red Persistent Luminescence Phosphor: The Example of YPO_4:Pr^{3+},Ln^{3+} (Ln = Nd, Er, Ho, Dy). *Journal of Physical Chemistry C*. 2011;115(10):4217-4227.

13. Yi GS, Chow GM. Synthesis of Hexagonal-Phase $NaYF_4$:Yb,Er and $NaYF_4$:Yb,Tm Nanocrystals with Efficient Up-Conversion Fluorescence. *Advanced Functional Materials*. 2006;16(18):2324-2329.

14. Stouwdam JW, van Veggel FCJM. Improvement in the Luminescence Properties and Processability of LaF_3/Ln and $LaPO_4$/Ln Nanoparticles by Surface Modification. *Langmuir*. 2004;20(26):11763-11771.

15. Wang F, Wang J, Liu XG. Direct Evidence of a Surface Quenching Effect on Size-Dependent Luminescence of Upconversion Nanoparticles. *Angewandte Chemie*. 2010;49(41):7456-7460.

16. Dong C, Korinek A, Blasiak B, Tomanek B, van Veggel FCJM. Cation Exchange: A Facile Method To Make $NaYF_4$:Yb,Tm-$NaGdF_4$ Core-Shell Nanoparticles with a Thin, Tunable, and Uniform Shell. *Chemistry of Materials*. 2012;24(7):1297-1305.

17. Abel KA, Boyer JC, van Veggel FCJM. Hard Proof of the $NaYF_4$/$NaGdF_4$ Nanocrystal Core/Shell Structure. *Journal of the American Chemical Society*. 2009;131(41):14644-14645.

18. Abel KA, Boyer JC, Andrei CM, van Veggel FCJM. Analysis of the Shell Thickness Distribution on $NaYF_4$/$NaGdF_4$ Core/Shell Nanocrystals by EELS and EDS. *Journal of Physical Chemistry Letters*. 2011;2(3):185-189.

19. Parchur AK, Prasad AI, Ansari AA, Rai SB, Ningthoujam RS. Luminescence properties of Tb^{3+}-doped $CaMoO_4$ nanoparticles: annealing effect, polar medium dispersible, polymer film and core-shell formation. *Dalton Transactions*. 2012;41(36):11032-11045.

20. Ansari AA, Yadav R, Rai SB. Influence of surface coating on structural, morphological and optical properties of upconversion-luminescent LaF_3:Yb/Er nanoparticles. *Applied Physics A*. 2016;122:635.

21. Ansari AA, Yadav R, Rai SB. Enhanced luminescence efficiency of aqueous dispersible $NaYF_4$:Yb/Er nanoparticles and the effect of surface coating. *RSC Advances*. 2016;6(26):22074-22082.

22. Ansari AA, Parchur AK, Kumar B, Rai SB. Influence of Shell Formation on Morphological Structure, Optical and Emission Intensity on Aqueous Dispersible $NaYF_4$:Ce/Tb Nanoparticles. *Journal of Fluorescence*. 2016;26(4):1151-1159.

23. Ansari AA, Parchur AK, Alam M, Azzeer A. Structural and photoluminescence properties of Tb-doped $CaMoO_4$ nanoparticles with sequential surface coatings. *Materials Chemistry and Physics*. 2014;147(3):715-721.

24. Ansari AA, Parchur AK, Alam M, Azzeer A. Effect of surface coating on optical properties of Eu^{3+}-doped $CaMoO_4$ nanoparticles. *Spectrochimica Acta Part A: Molecular and Biomolecular Spectroscopy*. 2014;131:30-36.

25. Ansari AA, Alam M, Parchur AK. Nd-doped calcium molybdate core and particles: synthesis, optical and photoluminescence studies. *Applied Physics A*. 2014;116(4):1719-1728.

26. Guo H, Li ZQ, Qian HS, Hu Y, Muhammad IN. Seed-mediated synthesis of $NaYF_4$:Yb, Er/$NaGdF_4$ nanocrystals with improved upconversion fluorescence and MR relaxivity. *Nanotechnology*. 2010;21(12):125602.

27. Ye S, Chen GY, Shao W, Qu JL, Prasad PN. Tuning upconversion through a sensitizer/activator-isolated $NaYF_4$ core/shell structure. *Nanoscale*. 2015;7(9):3976-3984.

28. Shen J, Chen GY, Ohulchanskyy TY, Kesseli SJ, Buchholz S, Li ZP, et al. Tunable Near Infrared to Ultraviolet Upconversion Luminescence Enhancement in (α-$NaYF_4$:Yb,Tm)/CaF_2 Core/Shell Nanoparticles for In situ Real-time Recorded Biocompatible Photoactivation. Small. 2013;9(19):3213-3217.

29. Mech A, Karbowiak M, Kepinski L, Bednarkiewicz A, Strek W. Structural and luminescent properties of nano-sized $NaGdF_4$:Eu^{3+} synthesised by wet-chemistry route. *Journal of Alloys and Compounds*. 2004;380(1-2):315-320.

30. Zhu HL, Ou GF, Gao LH. Hydrothermal synthesis of $LaPO_4$:Ce^{3+},Tb^{3+}@$LaPO_4$ core/shell nanostructures with enhanced thermal stability. *Materials Chemistry and Physics*. 2010;121(3):414-418.

31. Xu ZH, Yang J, Hou ZY, Li CX, Zhang CM, Huang SS, et al. Hydrothermal synthesis and luminescent properties of Y_2O_3:Tb^{3+} and Gd_2O_3:Tb^{3+} microrods. *Materials Research Bulletin*. 2009;44(9):1850-1857.

32. Wang CY, Cheng XH. Hydrothermal Synthesis and Upconversion Properties of α-$NaYF_4$:Yb^{3+}, Er^{3+} Nanocrystals Using Citric Acid as Chelating Ligand and NaNO3 as Mineralizer. *Journal of Nanoscience and Nanotechnology*. 2015;15(12):9656-9664.

33. Sun JY, Zhang WH, Du HY, Yang ZP. Hydrothermal synthesis and the enhanced blue upconversion luminescence of $NaYF_4$:Nd^{3+},Tm^{3+},Yb^{3+}. *Infrared Physics & Technology*. 2010;53(5):388-391.

34. Vetrone F, Naccache R, Mahalingam V, Morgan CG, Capobianco JA. The Active-Core/Active-Shell Approach: A Strategy to Enhance the Upconversion Luminescence in Lanthanide-Doped Nanoparticles. *Advanced Functional Materials*. 2009;19(18):2924-2929.

35. Liu DM, Zhao D, Zhang DS, Zheng KZ, Qin WP. Synthesis and Characterization of Upconverting $NaYF_4$:Er^{3+}, Yb^{3+} Nanocrystals via Thermal Decomposition of Stearate Precursor. *Journal of Nanoscience and Nanotechnology*. 2011;11(11):9770-9773.

36. Li W, Lee J. Microwave-Assisted Sol-Gel Synthesis and photoluminescence Characterization of $LaPO_4$: Eu^{3+},Li^{+} Nanophosphors. *Journal of Physical Chemistry C*. 2008;112(31):11679-11684.

37. Karvianto, Chow GM. The effects of surface and surface coatings on fluorescence properties of hollow $NaYF_4$:Yb,Er upconversion nanoparticles. *Journal of Materials Research*. 2011;26(1):70-81.

38. Karbowiak M, Mech A, Bednarkiewicz A, Stręk W, Kępiński L. Comparison of different $NaGdF_4$:Eu^{3+} synthesis routes and their influence on its structural and luminescent properties. *Journal of Physics and Chemistry of Solids*. 2005;66(6):1008-1019.

39. Ansari AA, Alam M, Labis JP, Alrokayan SA, Shafi G, Hasan TN, et al. Luminescent mesoporous $LaVO_4$:Eu^{3+} core-shell nanoparticles: synthesis, characterization, biocompatibility and their cytotoxicity. *Journal of Materials Chemistry*. 2011;21(48):19310-19316.

40. Ansari AA, Singh SP, Singh N, Malhotra BD. Synthesis of optically active silica-coated NdF_3 core-shell nanoparticles. *Spectrochimica Acta Part A: Molecular and Biomolecular Spectroscopy*. 2012;86:432-436.

41. Sayed FN, Grover V, Sudarsan V, Pandey BN, Asthana A, Vatsa RK, et al. Multicolored and white-light phosphors based on doped GdF_3 nanoparticles and their potential bio-applications. *Journal of Colloid and Interface Science*. 2012;367(1):161-170.

42. Ansari AA, Hasan TN, Syed NA, Labis JP, Parchur AK, Shafi G, et al. In-vitro cyto-toxicity, geno-toxicity, and bio-imaging evaluation of one-pot synthesized luminescent functionalized mesoporous SiO_2@$Eu(OH)_3$ core-shell microspheres. *Nanomedice*. 2013;9(8):1328-1335.

43. Ansari AA, Labis JP, Alrokayan SAH. Synthesis of water-soluble luminescent $LaVO_4$:Ln^{3+} porous nanoparticles. *Journal of Nanoparticle Research*. 2012;14:999.

44. Ansari AA, Labis JP. One-pot synthesis and photoluminescence properties of luminescent functionalized mesoporous SiO_2@$Tb(OH)_3$ core-shell nanospheres. *Journal of Materials Chemistry*. 2012;22(32):16649-16656.

45. Tauc J, Menth A. States in the gap. *Journal of Non-Crystalline Solids*. 1972;8-10:569-585.

46. Tao F, Pan F, Wang ZJ, Cai WL, Yao LZ. Synthesis and photoluminescence properties of hexagonal Lanthanide(III)-doped $NaYF_4$ microprisms. *CrystEngComm*. 2010;12(12):4263-4267.

47. Zhang ZJ, ten Kate OM, Delsing A, van der Kolk E, Notten PHL, Dorenbos P, et al. Photoluminescence properties and energy level locations of RE3+ (RE = Pr, Sm, Tb, Tb/Ce) in $CaAlSiN_3$ phosphors. *Journal of Materials Chemistry*. 2012;22(19):9813-9820.

48. Liu TC, Cheng BM, Hu SF, Liu RS. Highly Stable Red Oxynitride beta-SiAlON:Pr^{3+} Phosphor for Light-Emitting Diodes. *Chemistry of Materials*. 2011;23(16):3698-3705.

49. Li YC, Chang YH, Lin YF, Chang YS, Lin YJ. Luminescent properties of trivalent praseodymium-doped lanthanum aluminum germanate $LaAlGe_2O_7$. *Journal of Physics and Chemistry of Solids*. 2007;68(10):1940-1945.

50. Pellé F, Dhaouadi M, Michely L, Aschehoug P, Toncelli A, Veronesi S, et al. Spectroscopic properties and upconversion in Pr^{3+}:YF_3 nanoparticles. *Physical Chemistry Chemical Physics*. 2011;13(39):17453-17460.

51. Kar A, Patra A. Impacts of core-shell structures on properties of lanthanide-based nanocrystals: crystal phase, lattice strain, downconversion, upconversion and energy transfer. *Nanoscale*. 2012;4(12):3608-3619.

52. Yang PP, Quan ZW, Li CX, Yang J, Wang H, Liu XM, et al. Fabrication and luminescent properties of the core-shell structured $YNbO_4$: Eu^{3+}/Tb^{3+}@SiO_2 spherical particles. *Journal of Solid State Chemistry*. 2008;181(8):1943-1949.

53. Wang ZJ, Wu L, Liang HJ, Cai W, Zhang ZG, Jiang ZH. Controllable synthesis of bifunctional $NaYF_4$:Yb^{3+}/Ho^{3+}@SiO_2/Au nanoparticles with upconversion luminescence and high X-ray attenuation. *Journal of Alloys and Compounds*. 2011;509(37):9144-9149.

54. Wang Y, Qin WP, Zhang JS, Cao CY, Zhang JS, Jin Y. Synthesis and Upconversion Luminescence of LaF_3 : Yb^{3+}, Er^{3+}/SiO_2 Core/Shell Microcrystals. *Journal of Rare Earths*. 2007;25(5):605-608.

55. Szczeszak A, Ekner-Grzyb A, Runowski M, Szutkowski K, Mrówczynska L, Kazmierczak Z, et al. Spectroscopic, structural and in vitro cytotoxicity evaluation of luminescent, lanthanide doped core@shell nanomaterials $GdVO_4$:Eu^{3+} 5%@SiO_2@NH_2. *Journal of Colloid and Interface Science*. 2016;481:245-255.

56. Sivakumar S, Diamente PR, van Veggel FCJM. Silica-Coated Ln^{3+}-doped LaF_3 Nanoparticles as Robust Down- and Upconverting Biolabels. *Chemistry - A European Journal*. 2006;12(22):5878-5884.